February 2007

Effect of surrounding point charges on the density functional calculations of Ni_xO_x clusters (x = 4–12)

Evgueni B. Kadossov
University of Nebraska - Lincoln

Karen J. Gaskell
University of Nebraska - Lincoln

Marjorie Langell
University of Nebraska - Lincoln, mlangell1@unl.edu

Published in *Journal of Computational Chemistry* 28:7 (2007), pp. 1240–1251; doi: 10.1002/jcc.20669

Submitted August 1, 2006; revised October 29, 2006; accepted December 2, 2006; published online February 13, 2007.

Effect of surrounding point charges on the density functional calculations of Ni_xO_x clusters (x = 4–12)

Evgueni B. Kadossov, Karen J. Gaskell, Marjorie A. Langell*

Department of Chemistry, University of Nebraska–Lincoln, Lincoln, Nebraska 68588-0304

* *Correspondence*—Marjorie A. Langell, Department of Chemistry, University of Nebraska–Lincoln, Lincoln, Nebraska 68588-0304; email: mlangell@unlserve.unl.edu

Abstract

Embedded Ni_xO_x clusters (x = 4–12) have been studied by the density-functional method using compensating point charges of variable magnitude to calculate the ionic charge, bulk modulus, and lattice binding energy. The computations were found to be strongly dependent on the value of the surrounding point charge array and an optimum value could be found by choosing the point charge to reproduce the experimentally observed Ni–O lattice parameter. This simple, empirical method yields a good match between computed and experimental data, and even small variation from the optimum point charge value produces significant deviation between computed and measured bulk physical parameters. The optimum point charge value depends on the cluster size, but in all cases is significantly less than ±2.0, the formal oxidation state typically employed in cluster modeling of NiO bulk and surface properties. The electronic structure calculated with the optimized point charge magnitude is in general agreement with literature photoemission and XPS data and agrees with the presently accepted picture of the valence band as containing charge-transfer insulator characteristics. The orbital population near the Fermi level does not depend on the cluster size and is characterized by hybridized Ni 3d and O 2p orbitals with relative oxygen contribution of about 70%.

Keywords: nickel oxide clusters, point charge embedding, density-functional methods, electronic structure, ab initio calculations

Funded by National Science Foundation, Grant Number: CHE-0213320; Nebraska Research Initiative, State of Nebraska

Introduction

The electronic structure of NiO has been under active investigation for almost 6 decades, dating from the historic studies of Neville Mott,[1–3] which explained the insulating nature of the partially filled Ni^{2+} 3d level with a localized, antiferromagnetically ordered conduction band. Subsequent refinements produced the Mott-Hubbard model,[4][5] in which an insulating gap of energy U forms within the 3d level due to the strong Coulomb repulsion among the highly correlated 3d electrons. NiO was considered a prototypical Mott-Hubbard insulator for quite some time until the model was challenged by a series of photoemission experiments,[6][7] supported by ab initio cluster calculations,[8] which proposed the insulating nature originated from hybridization between localized nickel 3d and oxygen 2p levels. The band structure in this charge-transfer model is described by inclusion of configurations that transfer electron density between the filled O 2p[6] band into the empty Ni 3d:

$$\Psi_{\text{band}} = \alpha 3d^8 + \beta 3d^9 L + \gamma 3d^{10} L^2 \quad (1)$$

where, L represents a hole in the oxygen 2p band. The charge-transfer model explains satellite structure in photoemission quite well, but is less satisfactory in describing the composition of the top of the valence band and bottom of the conduction band, and thus the nature of the band gap. These problems occasionally give rise to a new round of controversy,[9-13] and the presently adopted picture of the NiO band structure often includes both Mott-Hubbard and charge-transfer nature.

As a theoretical understanding of the electronic nature of nickel oxide and other rocksalt 3d monoxides has developed, it has become apparent that in many cases computational methods have proven inadequate to describe key features of the band structure. In particular, ab initio studies of nickel oxide, especially those employing DFT methods, often fail to correctly describe the band gap, found experimentally to be in the range of 3.5-4.3 eV.[14–18] Many calculations either significantly underestimate the value at less than 1 eV,[19][20] or strongly overestimate it at greater than 4.5 eV.[21-25]

While the controversy over the nature of the band gap is fundamental, there is reason to believe that some inaccuracies in

calculations of NiO electronic properties are directly related to practical problems in the application of the DFT ab initio methods, illustrated by recent theoretical studies of adsorption on the NiO surface, a localized phenomenon for which cluster calculations should be particularly relevant. These results show that calculated geometric and energetic parameters for chemisorbed CO, NO, and NH_3 on NiO(100) are in poor agreement with experimentally observed data.[26][27] Even with directed efforts made to address this problem, the agreement in adsorbate geometry between calculation and experiment remains disappointing.[28–30] In nonperiodic studies, NiO is usually modeled as a cluster with fixed geometric parameters and surrounded by an array of point charges. For NiO, in which the ions are formally Ni^{2+} and O^{2-}, the point charges are usually taken at $q = \pm 1.8$ to 2.0 and, fundamentally, the array is employed to compensate for the Madelung potential of the lattice adjusted for effects that are related to the finite cluster size.[31]

Early NiO cluster calculations were performed on "bare" NiO clusters, with $q = 0$. In these calculations, accuracy was often associated with a fortuitously good choice of cluster geometry and size. For example, a bare cluster calculation using the same computational protocol was shown to produce oxide lattice parameters comparable to experimental values for $2 \times 2 \times 2$ clusters, but overestimated the value for $4 \times 4 \times 4$ clusters by as much as 0.06 Å.[32][33] DFT computations using bare Ni_xO_x clusters[20] gave optimized Ni–O bond lengths that were significantly underestimated for NiO, Ni_2O_2, and Ni_4O_4 clusters, by 21, 14, and 5.5%, respectively, and a calculated energy gap of 0.67–1.46 eV, seriously underestimating the experimental band gap value by as much as 3.6 eV. Semiempirical MSINDO studies employing $4 \times 4 \times 4$, $4 \times 4 \times 8$, $8 \times 8 \times 4$ and $8 \times 8 \times 8$ NiO[23] clusters resulted in consistently better agreement with experimentally determined lattice parameters and adsorbate binding energies, but still failed to model the observed band gap, overestimating it as 5.9–7.2 eV, depending on the cluster size and approach.

Compensation for the bulk crystal Madelung potential with an array of embedding point charges improves the accuracy of the cluster model, although care must be taken not to confuse the charge magnitude ($\pm q$) of bare, unshielded point charges that best represent the Madelung potential of the lattice with the charge on ions that compose it. The point charges also do not participate directly in bonding, but merely provide a background to compensate for the lattice Coulomb potential on the cluster. The relationship between the magnitude of the point charge and that of the lattice ion formal charge is not obvious, and the use of $q = \pm 2.0$ is not necessarily the best choice to reproduce the actual chemical environment of the cluster in the three dimensional structure of the bulk lattice.

Both geometric and energetic properties of nickel oxide dimer clusters[34] have been shown to depend strongly on the magnitude of the surrounding point charges. In this case, the point charge was varied over a range of $q = 0$ to ± 2.0, with a point charge value of ± 1.36 most accurately reproducing the Ni–O bond length observed in the bulk crystal structure. However, the optimization of NiO clusters larger than dimer size, particularly in relation to point charge values, can lead to convergence problems and have not been studied in depth.

The point charge value used to construct the array also affects computational results involving chemisorbed species. A strong correlation between point charge array and energy characteristics has been found in embedded NiO cluster calculations[35] used to model the electronic structure for CO adsorbed on the NiO(100) surface, which was observed to vary significantly when the point charge was varied over the relatively narrow range of $q = \pm 1.72$ to 2.00. These studies indicate that point charge optimization should be taken into account when performing calculations of both NiO bulk and surface properties.

For the related MgO system, a number of cluster calculations have been performed that question the validity of using the formal lattice ion oxidation states for the point charge value, even for highly ionic metal oxide systems. Calculations that model MgO(100) chemisorption[36–43] indicate that a point charge of ±2.0 significantly overestimates the effect of the surrounding MgO crystal on adsorbate bonding and energetics. The majority of these studies limited their calculations to a single value of q, generally either $q = \pm 1.5$ or ± 1.8,[38–41] and did not systematically investigate the effect of point charge on chemisorption properties. However, when specific efforts were made to determine an optimum value for q in DFT cluster calculations, it was found to be significantly less than the formal oxidation state. For example, Mg_xO_x cluster calculations modeling the interaction of CO[42] and Cl_2[43] with MgO(100) used a spherically expanded point charge model (SPC)[34] to optimize q self-consistently, and the point charge for these systems was determined to be in the range of $q = \pm 0.85$ to 1.04, depending upon cluster size.

In this work, we perform ab initio DFT optimizations of Ni_xO_x clusters ($x = 4$–12) embedded in a point charge field and study the correlation between the electronic properties of the NiO clusters and the value of the surrounding point charges. We show that a simple and convenient method of selecting a reasonable point charge value is by choosing q empirically to reproduce the bulk NiO lattice parameter upon cluster Ni–O bond optimization. Point charge arrays with this optimized q value are shown to yield acceptable results for bulk crystal properties, including band gap and other electronic properties. Using this approach, the lattice binding energy and bulk modulus have been calculated for each cluster size and compared to their experimentally observed bulk values. The electronic band structure of both ferromagnetic and antiferromagnetic NiO is analyzed and discussed in light of the currently accepted picture.

Computational Procedure

Cluster calculations were performed using Gaussian03W software.[44] For cluster optimization, the density-functional method with Beck three-parameter hybrid and Lee-Yang-Parr exchange functionals (B3LYP) was applied.[45][46] Nickel cation wavefunctions were modeled with a LanL2DZ basis set, which combines the D95V[47] double-zeta functions with Los-Alamos effective core potentials (ECP).[48] For oxygen anions, the 6-31G* all-electron split-valence basis set[49] was used and included a polarization d-function. Geometry optimization was performed with the eigenvalue-following algorithm (EF)[50–52] by varying the lattice parameter a (Ni–O bond length) while fixing

all bond angles at 90° in an undistorted rock-salt structure. Ni_xO_x structures were treated as both ferromagnetic and antiferromagnetic, since the ground state of solid NiO is antiferromagnetic AF_2 below the Néel temperature of 525 K.[53] Population analysis was performed with the help of the natural bond analysis (NBO) utility built into the Gaussian software.

The criteria for cutting-out embedded clusters[54] require that the clusters should be neutral, stoichiometric and have a minimum amount of dangling bonds. The clusters used in this work have been chosen to satisfy these requirements. The nickel oxide solid is represented by a series of Ni_xO_x clusters with x = 4–12 (Fig. 1), embedded in an array of alternating positive and negative point charges of equal magnitude. The point charge array is constructed by surrounding the cluster ions with four layers of point charges (4 layers deep), corresponding to a net 10 × 10 × 10 system in the case of Ni_4O_4, 10 × 11 × 10 for Ni_6O_6, 10 × 12 × 10 for Ni_8O_8, 11 × 11 × 10 for Ni_9O_9, 10 × 13 × 10 for $Ni_{10}O_{10}$, and 11 × 12 × 10 for $Ni_{12}O_{12}$. All point charges are situated at the normal crystallographic lattice coordinates, keeping the distance between neighbor charges fixed at the experimental NiO lattice parameter of 2.084 Å.[55]

For comparison purpose, periodic DFT calculations have been performed on ferromagnetic and antiferromagnetic NiO using the spin unrestricted B3LYP hybrid density functional implemented with the CRYSTAL98 package.[56][57] Supercells containing four atoms (2 Ni and 2 O) were used in both ferromagnetic and antiferromagnetic (AF_2) calculations. Electron basis sets of the form 86-411/41 for nickel and 84-11 for oxygen were adopted from previous crystal calculations.[53] Even tempered auxiliary basis sets shown to yield good results in a previous study[58] were used for fitting the exchange correlation potential, and comprised 14 s-type functions with exponents between 0.07 and 4000 for oxygen, 12 s-type functions with exponents between 0.1 and 6,000 for nickel, and 3d-type type functions with exponents between 0.45 and 3.3 for nickel. To keep numerical error in the DFT part of the calculation to a minimum, the accuracy of the angular numerical integration during the SCF stage of the calculation was increased to the default level used in the exchange-correlation energy estimation and for the radial integration the number of points in the radial quadrature was increased to 81. The accuracy of the calculation of the bielectronic Coulomb and exchange series are controlled by 5 ITOL parameters which were set to high levels: 7, 7, 7, 7, and 14. The SCF thresholds for the eigenvalues and total energy were set to 7 and 6, respectively. Fock/KS matrix mixing of 30% was used to aid with convergence. Geometry optimizations were performed utilizing the FIXINDEX option by carrying out 11 single-point calculations, varying the unit cell lattice constant between 4.10 and 4.32 Å at intervals of 0.02 Å, the theoretical lattice constant was obtained by fitting a fourth order polynomial to the total energies. Calculations presented were carried out at the theoretical lattice constants, which were 4.24 and 4.23 Å for the ferromagnetic and antiferromagnetic NiO systems, respectively.

Results and Discussion

Bulk Parameters

Ferromagnetic Ni_4O_4 Cluster

The effect of the point charge was first investigated for the smallest embedded cluster, Ni_4O_4, in its ferromagnetic configuration. In addition, the lattice binding energy E_{lat} and the bulk modulus B were calculated as a function of point charge over the range of values q = 0 to ±2.0. The lattice binding energy is defined as that required to convert:

$$NiO_{(s)} \rightarrow Ni_{(g)} + O_{(g)} \quad (2)$$

and the results can be compared with the experimentally observed value for NiO of 8.8 eV (849 kJ/mol).[32] The bulk modulus was estimated with the equation[33]:

(3)

where k is the harmonic force constant for isotropic compression of the cluster and a is the equilibrium separation between nearest Ni–O neighbors. The model assumes that the energy varies harmonically in the vicinity of a.

The results obtained are summarized in Table1. The average atomic charges have been calculated in two ways: as Q_M, the Mulliken charge, computed during the lattice parameter optimization and as Q_N, the natural charge, obtained by the NBO analysis procedure. As expected, with no point charge array the bare ferromagnetic cluster calculations poorly reproduce bulk NiO properties. Under these conditions, the optimized lattice parameter is calculated to be 1.940 Å, differing from the experimental value by 0.14 Å. The lattice parameter a used here is the Ni–O nearest neighbor distance and is equal to one half the rocksalt unit cell length. The bulk modulus calculated for this system is overestimated at 3.46 × 10^{12} dyn/cm^2, twice that observed experimentally. The lattice energy E_{lat} = 610 kJ/mol is underestimated by about 28%.

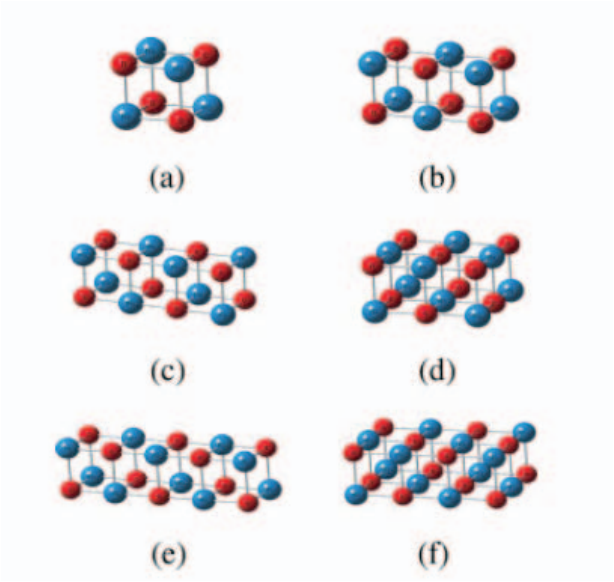

Figure 1. Ni_xO_x cluster models (a) x = 4, (b) x = 6, (c) x = 8, (d) x = 9, (e) x = 10, (f) x = 12.

Table 1. Calculated Lattice Parameter a (Å), Bulk Modulus B (10^{12} dyn/cm^2), Lattice Energy (kJ/mol), and Average Mulliken and Natural Charges on Ni and O Ions in the Ferromagnetic Ni_4O_4 Cluster at Different Values of Surrounding Point Charge q.

q	a	B	E_{lat}	Q_M	Q_N
0.0	1.940	3.46	610	0.74	1.14
0.5	2.011	2.92	805	0.86	1.33
0.7	2.056	2.56	903	0.91	1.40
0.75	2.070	2.45	928	0.93	1.42
0.795	2.084	2.32	952	0.94	1.43
1.0	2.178	1.40	1075	0.99	1.50
1.5	2.887	1.06	1566	1.27	1.61
2.0	2.084 (fixed)	2.03	1717	1.28	1.69
Experiment	2.084[a]	1.73 ± 0.23[b]	849[c]		

[a] Ref.[55].
[b] Ref.[59].
[c] Ref.[32].

Embedding the cluster in a field of point charges significantly improves the agreement between calculated and experimentally observed properties. As q is increased, the Ni–O lattice parameter a and lattice energy E_{lat} both increase while the bulk modulus B decreases. For the ferromagnetic Ni_4O_4 cluster, the lattice parameter becomes equal to the experimental value of 2.084 Å at a point charge value of $q = \pm 0.795$. At this value, E_{lat} and B are within reasonable agreement of their experimental value as well. The optimized point charge value varies only slightly with reasonable choice of basis sets. Substituting 6-311G+ for the 6-31G* oxygen basis set returns $q = \pm 0.720$ as an optimum value, whereas replacing the nickel LanL2DZ basis set with 6-31G* increases it to $q = \pm 0.845$. Further increase in q results in overestimation of a and an increasingly poor agreement of E_{lat} and B with their observed bulk value. For $q = 1.5$, still significantly below the formal charge of $q = 2.0$, the lattice parameter a is 2.887 Å, or approximately 40% higher than the experimentally observed value.

At $q = 2.0$, convergence problems arise due to the enormously high Madelung potential represented by the point charge field and an optimized lattice parameter cannot be obtained. However, the bulk modulus and lattice energy can be calculated by assuming a Ni–O bond length of 2.084 Å, equal to that observed experimentally. While this assumption produces a reasonable value for the bulk modulus, the calculated lattice energy is more than twice the experimental value. Furthermore, frequency analysis, described below, results in the appearance of imaginary modes during the optimization of the lattice parameter for $q \geq 1.5$, indicating instability in the calculation of the embedded cluster. No imaginary frequencies were observed in the lattice optimization for Ni_4O_4 clusters with $q \leq 1.0$.

The average ionic charge also shows strong dependence on the embedded point charge value. While Q_N calculations produce larger values than those using Q_M, all are consistently well below the formal charge of 2.0. Mulliken analysis tends to underestimate charge calculations for ionic systems more severely because it divides shared electron density in overlap terms evenly between the two ions whereas NBO analysis distributes the overlap density by summing predefined "natural" atomic orbital assignments. Both Q_M and Q_N are clearly proportional to q, although both also clearly underestimate the actual charge and the discrepancy is typical of that for charge calculations of strongly ionic systems by density functional methods. For example, in periodic DFT studies of the NiO lattice, the calculated atomic charge has typically been reported to lie within ±1.53 to 1.67, while SCF calculations on the same system produce more reasonable values in the range of 1.8-1.9.[58] The large difference between the charge distribution calculated by DFT and SCF methods has been well recognized in the literature and is a result of the protocol for assigning electron density among shared, valence-level electrons.[60] While the charge calculations are known to underestimate the atomic charge, they produce reasonable trends in comparing charge variation for systems using the same computational protocols.

To ensure a large enough point charge array had been chosen in the present calculations to make them independent of array size, the effect of the array size was studied for the Ni_4O_4 cluster by embedding it in a field comprised of a larger, 20 × 20 × 20 array. The optimized lattice parameter a was found to be equal to that calculated with 10 × 10 × 10 array with the same optimized q value, while the lattice energy differed from that shown in Table 1 for the 10 × 10 × 10 array by only several kJ/mol. Therefore, the 10 × 10 × 10 point charge array was employed in the remainder of the calculations and is assumed to be large enough to satisfactorily simulate the Madelung potential of the lattice.

Optimized Ni_xO_x Clusters

Below its Néel temperature of 525 K,[61] bulk nickel oxide is antiferromagnetic in AF_2 form with ordered spin-up (α) and spin-down (β) electrons in alternating (111) nickel planes. Optimized point charge values calculated for the spin-paired Ni_xO_x (x = 4–12) embedded clusters are given in Table2, where q is calculated to reproduce the experimentally observed nickel oxide lattice parameter, as described earlier. Figure 2 shows the electron spin coupling schemes for Ni_6O_6 that reproduce the spin order of the ferromagnetic and AF_2 antiferromagnetic structures for

Table 2. Bulk Modulus B (10^{12} dyn/cm^2), Lattice Energy E_{lat} (kJ/mol), and Average Mulliken and Natural Charges on Ni and O Ions Calculated at Optimum Point Charge Value q for Antiferromagnetic (AF_2) Ni_xO_x (x = 4–12) Clusters.

X	***S***	***q***	***B***	E_{lat}	Q_M	Q_N
4	2	0.804	2.28	958	0.94	1.44
6	0	0.684	1.95	895	0.88	1.41
8	0	0.628	2.04	875	0.86	1.41
9	1	0.564	1.85	849	0.84	1.39
10	0	0.598	2.02	866	0.85	1.40
12	0	0.509	1.77	835	0.82	1.38

S, the total spin of the cluster.

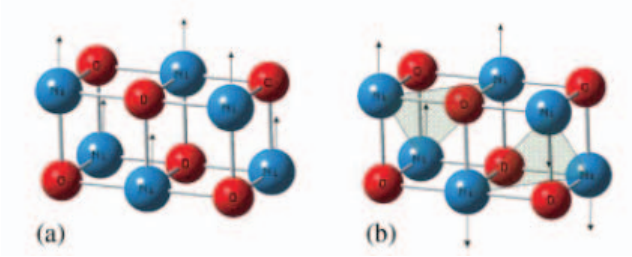

Figure 2. Ni_6O_6 cluster: (a) Ferromagnetic spin ordering, (b) AF_2 antiferromagnetic spin ordering. Semitransparent areas designate (111) planes of the same spin direction.

this cluster. Antiferromagnetic coupling can be included in the density functional calculations for some, but not all, of the clusters considered here and not all spin $S = 0$ systems can be configured to reproduce the antiferromagnetic AF_2 ordering observed in the bulk. The Ni_9O_9 cluster contains an odd number of nickel ions and cannot balance α and β spins completely, and the minimum spin AF_2 ordered system for this cluster is $S = 1$. While an $S = 0$ spin arrangement for the Ni_4O_4 cluster can be envisioned, the spins are incorrectly aligned for AF_2 antiferromagnetism. AF_2 spin ordering produces an $S = 2$ system for the cluster and is the cluster system used here. Finally, for the Ni_8O_8 system, an antiferromagetic AF_2 configuration with paired α and β spins ($S = 0$) can be formed, but the two spins are not symmetrically equivalent within the cluster. Thus, of the clusters considered here only the Ni_6O_6, $Ni_{10}O_{10}$, and $Ni_{12}O_{12}$ accurately represent the spin configuration for an antiferromagnetic AF_2 bulk material.

The results in Table 2 indicate that an increased cluster size requires a smaller value of the optimum point charge, with q varying from 0.804 for Ni_4O_4 to 0.509 for $Ni_{12}O_{12}$ among the clusters considered here. As the cluster size is increased, calculated values of both the bulk modulus and the lattice energy also improve and approach that observed experimentally, with excellent agreement achieved for the $Ni_{12}O_{12}$ cluster at its optimum q value. The average atomic charge changes insignificantly as the cluster size is increased and remains in the range 0.82–0.94 (Mulliken charge) or 1.38–1.44 (natural charge) for all clusters. The nonlinearity in x (cluster size) for calculated values of q, B, and E_{lat} is a function of cluster symmetry, and clusters are more accurate in reproducing bulk values if the cluster is more compact, which more efficiently increases the number of nearest-neighbors and decreases the number of dangling bonds.

For comparison to the AF_2 embedded cluster calculations, optimal point charge values for the ferromagnetic clusters are listed in Table3. Antiferromagnetically and ferromagnetically ordered Ni_xO_x clusters show similar trends in the manner in which bulk modulus and lattice energy improve with cluster size. However, the optimized point charge q values obtained in the ferromagnetic calculations are slightly smaller than those observed for their corresponding antiferromagnetic clusters, and the difference becomes greater with increased cluster size. The lattice energy is smaller by approximately 10 kJ/mol for the ferromagnetic clusters, consistent with other computational data.[23] The Mulliken and natural atomic charges and the bulk modulus values are comparable to those of the antiferromagnetic clusters and at constant q do not significantly change with the increased cluster size.

Electronic Structure

HOMO-LUMO Energy Gap

The HOMO-LUMO energy gap (E_g) calculated for a cluster is often taken to be a measure of the band gap of the bulk material.[62] Experimental values are generally measured optically, and the presently accepted value for the optical NiO band gap lies within the range of 3.5–4.3 eV.[7][18] The band gap of NiO is often poorly estimated by computational techniques, a problem compounded by the controversy over the composition of states at the top of the valence band (HOMO states) and the bottom of the conduction band (LUMO states). This is further exacerbated by difficulties in the measurement of the fundamental gap itself. NiO states in the band gap vicinity are predicted by the Mott-Hubbard model to be primarily of Ni 3d nature, whereas the charge-transfer insulator model predicts hybridized Ni 3d-O 2p states near the Fermi level at the top of the valence band. Since the bottom of the conduction band is primarily of Ni 3d nature, it has been proposed[10] that the optical measurements might overestimate the oxygen 2p hybridization at the top of the NiO valence band since the optical measurements favor $\Delta l = \pm 1$ transitions by dipole selection rules. While the maximum in the measured optical adsorption coefficient is found at about 4.3 eV, the spectrum has been reported to show a weak onset of absorption detectable as low as 3.1 eV[63] that could more potentially be associated with the computed HOMO-LUMO value of the energy gap, E_g.

Cluster calculations, performed with the optimum point charge values reported in Tables 2 and 3, were used to estimate the NiO band gap energy, E_g. The calculated E_g value, measured as the difference in energy between the bottom of the LUMO state and top of the HOMO state, is shown in Table4 as a function of cluster size for both ferromagnetic and antiferromagnetic clusters. The agreement with experiment is quite good. For all but the smallest cluster of $x = 4$, the calculated energy gap is comparable to or only a few tenths of an eV below that observed experimentally. The magnitude of E_g for each cluster is strongly dependent

Table 3. Bulk Modulus B (10^{12} dyn/cm^2), Lattice Energy E_{lat} (kJ/mol), and Average Mulliken and Natural Charges on Ni and O Ions Calculated at Optimum Point Charge Value q for Ferromagnetic Ni_xO_x (x = 4-12) Clusters.

X	*S*	*q*	*B*	E_{lat}	Q_M	Q_N
4	4	0.795	2.32	952	0.94	1.43
6	6	0.667	1.95	884	0.88	1.41
8	8	0.614	1.90	866	0.86	1.40
9	9	0.534	1.82	833	0.84	1.39
10	10	0.582	1.93	856	0.85	1.40
12	12	0.479	1.68	821	0.82	1.38

S, the total spin of the cluster.

Table 4. Energy Gap (eV) Between HOMO and LUMO for Ni_xO_x (x =4-12) Ferromagnetic and Antiferromagnetic (AF_2) Clusters Calculated at the Optimum Point Charge Value q Taken from Tables 2 and 3.

	Ferromagnetic clusters		Antiferromagnetic and minimum spin clusters[a]	
X	E_g (α)	E_g (β)	E_g (α)	E_g (β)
4	4.8	4.8	4.8	4.6
6	4.2	4.1	4.0	4.0
8	4.3	4.3	4.0	4.3
9	3.9	3.4	3.6	3.7
10	4.1	4.1	4.1	4.1
12	3.8	3.6	3.7	3.7

[a] x = 4 and 9 values taken for minimum value spin state of S = 1 and 2, respectively.

on q. For example, if the Ni–O bond length is fixed at the experimentally observed value (2.084 Å) and the formal charge (q = ±2.0) is used to construct the point charge array, as is typical practice in metal oxide cluster calculations, E_g is significantly overestimated and ranges from 5.2 to 6.7 eV, depending upon cluster size.

In both ferromagnetic and antiferromagnetic cases, E_g decreases slightly with cluster size, although the most substantial change occurs in going from the minimum cluster size of x = 4 to the next smallest at x = 6. The largest antiferromagnetic cluster studied here, $Ni_{12}O_{12}$, yields a value of E_g that is approximately 0.3–0.6 eV below the optical gap. In light of the trend of decreasing E_g with increasing cluster size, the slightly lower computed band gap value might be taken in support that optical measurements overestimate the energy gap of the material, and that the transition at the gap involves Ni 3d valence states into Ni 3d conduction states. However, population analysis described below shows that the embedded cluster calculations place significant O 2p character at the top of the valence band, in agreement with the charge-transfer insulator model of the band structure. The lower value for the calculated band gap value should, therefore, be taken as a measurement of the accuracy of the calculation in reproducing the observed optical band gap transition.

Cluster geometry is, again, a factor in the calculation. More compact clusters produce lower energy values in a trend similar to that observed for bulk modulus and lattice energy in which a slight trend reversal is observed in going from Ni_9O_9 to $Ni_{10}O_{10}$, since x = 9 produces a more compact cluster than x = 10. The difference between E_g for majority (α) and minority (β) electrons in Table 4 is also related to the cluster and spin-orbitals symmetry for the ferromagnetic and $S \neq 0$ AF_2 spin-paired NiO clusters. By symmetry, the bulk AF_2 antiferromagnetic α and β subbands are equivalent and yield equal E_g.

Band Structure and Population Analysis

The energy-level diagram representing the band structure of the Ni_6O_6 cluster is shown in Figure 3 for Ni 3s and higher levels. The overall picture of the band structure is as expected. The more strongly bound Ni 3s and Ni 3p core levels are localized and consist of unhybridized atomic nickel wavefunctions, and the O 2s wavefunctions form a shallow, localized core state approximately 12 eV below the bottom of the valence band. In both ferromagnetic and antiferromagnetic Ni_6O_6 clusters, higher energy states begin to show signs of admixture of other levels. While the Ni 3p band essentially contains only pure Ni 3p states, the next band separated from the Ni 3p level by approximately 50 eV, consists primarily of O 2s but contains a small amount of less than 7% Ni 3s and 3d character.

The NiO valence band almost exclusively consists of Ni 3d and O 2p atomic wavefunctions, with a small amount of O 2s and Ni 4s admixture. In the ferromagnetic Ni_6O_6 cluster, the band contains 48 α-spin and 36 β-spin orbitals, consistent with the experimental data and previous ab initio calculations.[8] Population analysis for majority-spin (α) electrons indicates that the top of the valence band contains a large amount of O 2p character (Fig. 4a). Although the nature of the top of the valence band remains controversial,[10][64-66] a large contribution by the O 2p to this region has been found both experimentally[10] and computationally by cluster[22][24] and periodic lattice methods.[53][58] The Ni 3d states dominate the bottom of the valence band but also show some contribution to the top of the valence band comprising about 30% of the total states within 1 eV of the Fermi level by population analysis. The low energy portion of the conduction band is primarily composed of minority (β) spins of Ni 3d character, with only a small contribution of O 2p (Fig. 4b). Since the minimum HOMO-LUMO transition involves minority spins (Table 4), the optical band gap transition is predominately p → d compatible with the $3d^{[8]}L \rightarrow 3d^{[9]}$ charge-transfer insulator model. Increasing the cluster size does not increase the amount of Ni 3d at the top of the valence band, as can be seen for the $N_{12}O_{12}$ cluster in Figure 5, where now 96 α-spin and 72 β-spin orbitals contribute to the valence and conduction bands.

Population analysis for antiferromagnetic Ni_6O_6 gives qualitatively the same picture (Fig. 6a), although the distribution of spin states is slightly different than observed for the ferromagnetic

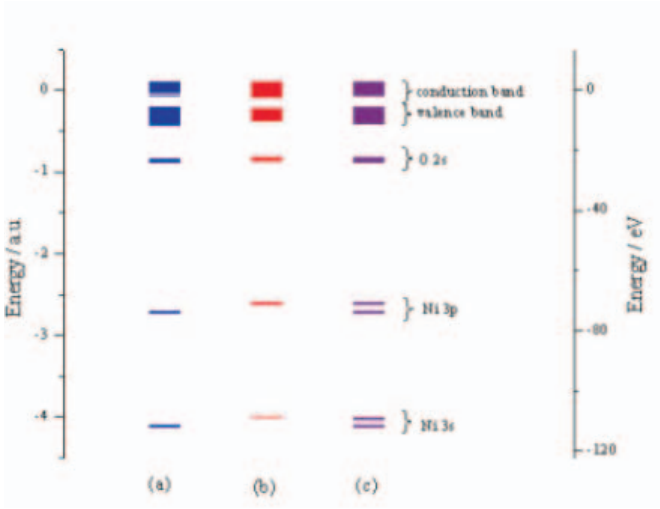

Figure 3. Molecular orbital band structure for the optimized Ni_6O_6 cluster: (a) α electrons in the ferromagnetic configuration; (b) β electrons in the ferromagnetic configuration; (c) α and β electrons in the antiferromagnetic configuration.

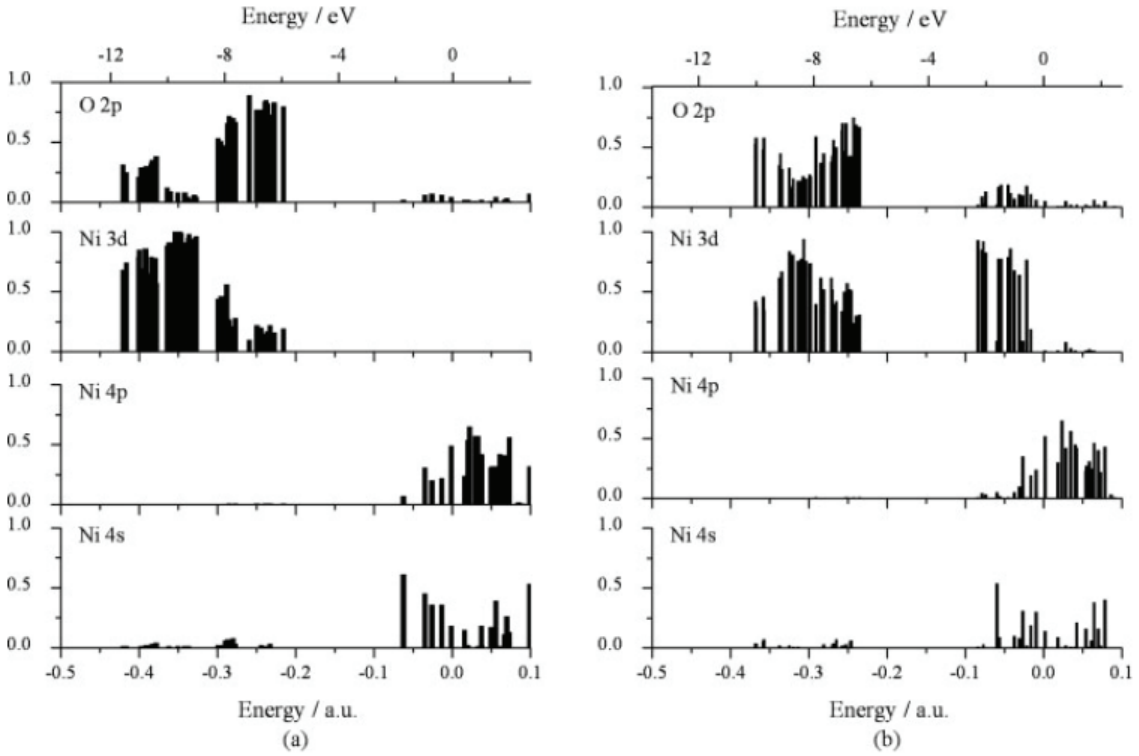

Figure 4. Population diagram for the (a) majority-spin α and (b) minority-spin β electrons in the valence and lower conduction band region of the optimized ferromagnetic Ni_6O_6 cluster.

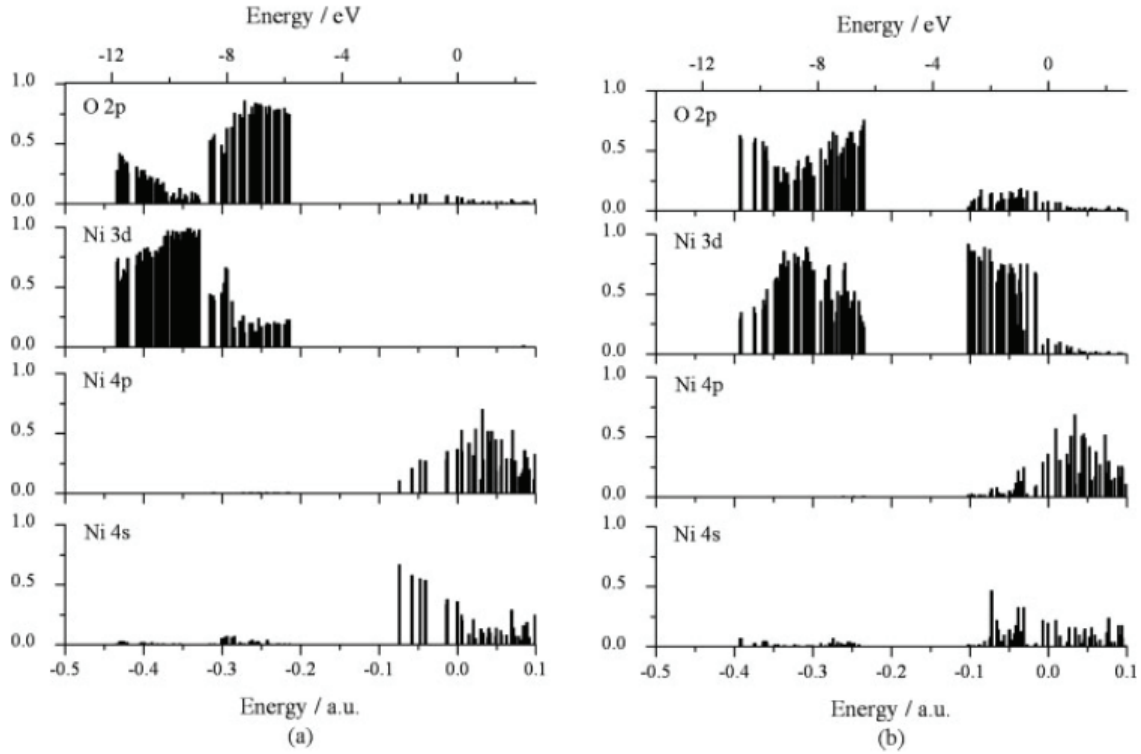

Figure 5. Population diagram for the (a) majority-spin α and (b) minority-spin β electrons in the valence and lower conduction band region of the optimized ferromagnetic $Ni_{12}O_{12}$ cluster.

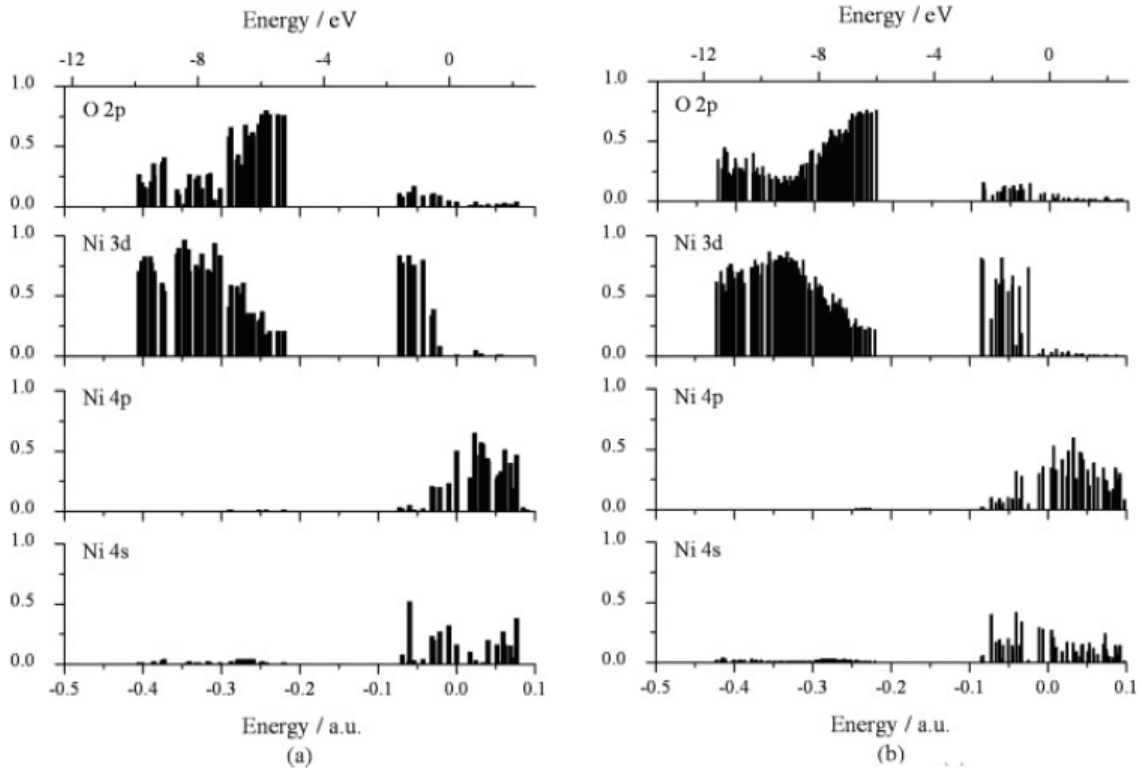

Figure 6. Population diagram for the majority-spin α and minority-spin β electrons in the valence and lower conduction band region of the optimized antiferromagnetic Ni_6O_6 (a) and $Ni_{12}O_{12}$ (b) clusters.

cluster. In clusters that accurately reproduce the AF_2 spin order, α and β bands are symmetrically equivalent and only one set is shown in Figure 6a. The upper part of the valence band is still dominated by the O 2p states at about 70% of the total number of states. The bottom of the conduction band is still predominately Ni 3d, but the admixture of O 2p is slightly greater. Again, increasing cluster size does not significantly change the picture (Fig. 6b).

To further illustrate the composition of the valence band edge, Table5 contains the numerical values from population analysis for the fraction of states with Ni 3d character within the upper 1 eV of the valence band for the series of Ni_xO_x embedded clusters. The remaining fraction is essentially all O 2p. The highest occupied α spin molecular orbital has been taken as the reference point for the top of the valence band. For all clusters, in both ferromagnetic and antiferromagnetic spin configurations, the O 2p orbitals can be clearly seen to dominate the top of the valence band. Increasing the cluster size does not change the population distribution of this region and the relative proportion of Ni 3d wavefunctions remains within 26–30% of the total number of states. However, the Ni 3d wavefunctions are distributed differently between the α and β subbands for ferromagnetic and antiferromagnetic clusters. In the ferromagnetic NiO system, Ni 3d electrons comprise ~15–20% of the top 1 eV of the majority α subband and ~34–42% to the minority β subband. For the antiferromagnetic clusters, the fraction of Ni 3d character is calculated to be ~27% in this highest 1 eV of the valence band and is equal for α and β subbands.

Density of States

Population analysis determines the fractional contribution of each orbital used in a calculation to each state, but does not represent the density of states $g(\varepsilon)$ within each energy value interval $d\varepsilon$. The density of states can be determined by:[33]

$$g(\varepsilon)d\varepsilon = \frac{n_\varphi}{V} \quad (4)$$

where V is the volume of the unit cell and n_φ is the number of one electron levels in the energy range ε to $d\varepsilon$. Since cluster calculations produce a relatively small number of molecular orbitals

Table 5. Relative Fraction of Ni 3d States in the Upper 1 eV of the Valence Band.

	Ferromagnetic			Antiferromagnetic and minimum spin clusters[a]		
X	***α***	***β***	**Total**	***α***	***β***	**Total**
4	0.15	0.41	0.28	0.18	0.36	0.27
6	0.18	0.40	0.29	0.26	0.26	0.26
8	0.18	0.41	0.30	0.26	0.27	0.27
9	0.19	0.34	0.26	0.25	0.26	0.26
10	0.18	0.42	0.30	0.26	0.26	0.26
12	0.20	0.38	0.29	0.27	0.27	0.27

[a] $x = 4$ and 9 values taken for minimum value spin state of $S = 1$ and 2, respectively.

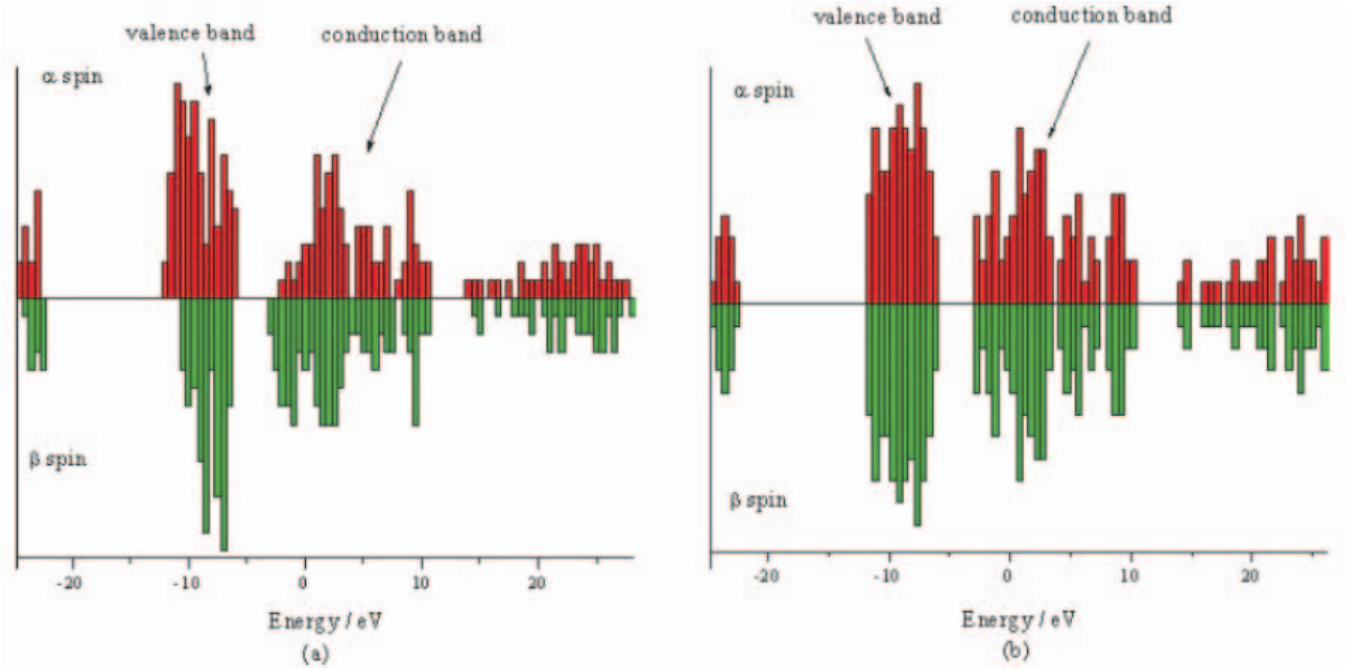

Figure 7. Density of states representation for the optimized (a) ferromagnetic and (b) antiferromagnetic $Ni_{12}O_{12}$ clusters.

with discrete energy values, the appropriate approximation for cluster calculations is to sum the number of states falling into a small energy interval, Δε. The normalizing volume V can be defined as the volume that contains one NiO diatomic cluster molecule since the primitive unit of a rocksalt lattice contains two atoms. Hence, in cluster calculations, the density of states can be obtained from the following relationship:

$$g(\varepsilon)\Delta\varepsilon = \frac{n_\varepsilon}{N} \tag{5}$$

where n_ε is the number of energy levels in the range ε to (ε + Δε) and N is the number of NiO units contained in the cluster (in the case of $Ni_{12}O_{12}$, $N = 12$).

The total DOS representations for the ferromagnetic and antiferromagnetic spin-ordered systems are depicted in Figure 7 for the $Ni_{12}O_{12}$ cluster. In both cases, Δε is taken to be equal 0.5 eV. The shape and the bandwidth of the valence and conduction bands are qualitatively compatible with the spectra obtained by XPS and BIS,[64] although satellite structure observed experimentally as a small shoulder approximately 6 eV below the Fermi level is not resolved in the summed-state DOS estimation. The absence of energy states in the bottom of the valence band that would give rise to this feature can be explained by the finite size of $Ni_{12}O_{12}$ cluster, which requires a fairly large Δε to avoid grainy DOS curves and does not estimate states with low intensity very well. The separation between the most intense DOS features composed of O 2s and O 2p wavefunctions is about 16 eV, reproducing the experimental value of 16 eV between O 2s and O 2p peak maxima observed in NiO XPS studies.[67]

Comparison of Cluster and Periodic DFT Calculations

Periodic DFT calculations have been performed on ferromagnetic and antiferromagnetic NiO supercells, as described in the computational procedure section above. The resulting total density of states for the two bulk structures is shown in Figure 8 in the range of the valence and lower conduction bands. The antiferromagnetic electronic band structure of NiO using B3LYP periodic methods have been reported in earlier studies, and the results presented here agree with those previously published.[58][68][69] To our best knowledge, there exists no previous studies that address the DOS of the ferromagnetic band structure using periodic B3LYP methods.

The band gap of the antiferromagnetic NiO is calculated to be 4.2 eV, in excellent agreement with optical measurements and only slightly higher than the 3.7 eV value of the $Ni_{12}O_{12}$ cluster calculated with the optimized embedded charge of $q = 0.509$. For the ferromagnetic system, separation between the top of the valence band and the bottom of the conduction band for the α (majority) spins is 3.8 eV and for the β (minority) spins is 3.2 eV, with the β transition underestimating the true band gap slightly more than does the cluster calculation. While band widths and relative positions are comparable for the cluster and periodic techniques, the shape of the valence and conduction bands differs somewhat, in part due to the limited number of states contributing to the cluster calculations. Nevertheless, the cluster results are within reasonable accuracy of the periodic calculations. The cluster calculations using our optimal point charge method for estimating the embedding point charge can, therefore, be taken as a significant improvement over previous cluster calculation methods in their agreement with periodic derived band gap values.

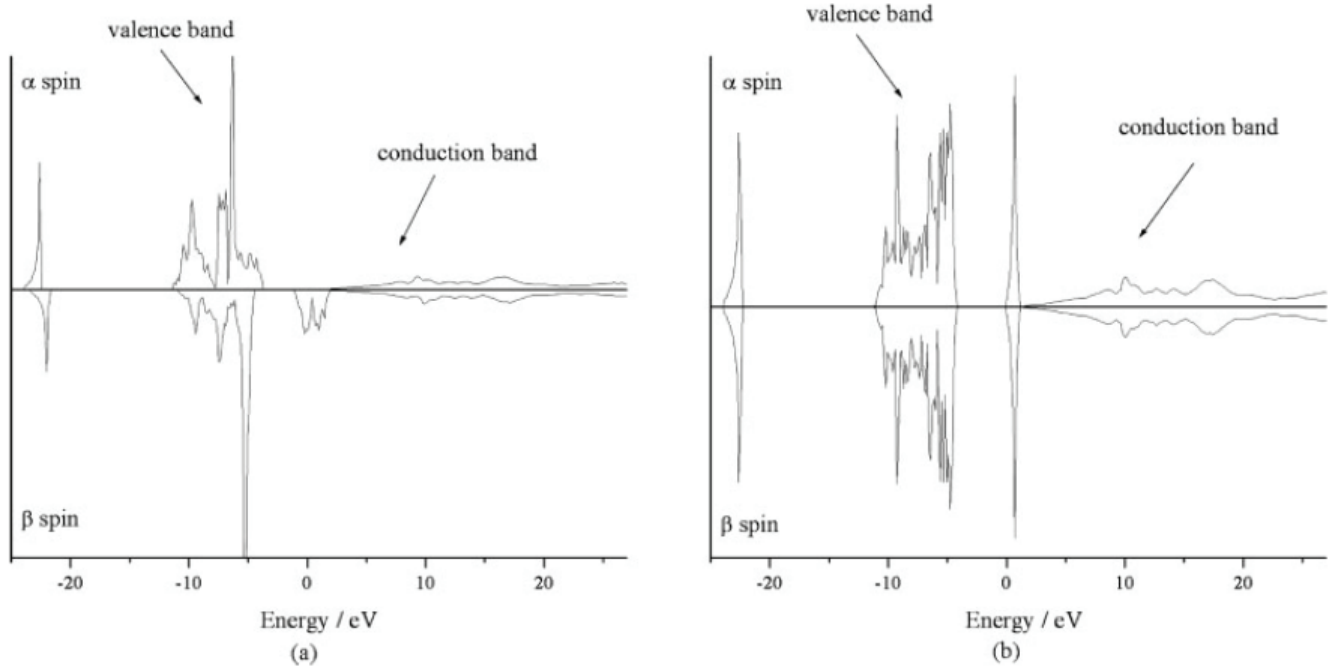

Figure 8. Total density of states for optimized (a) ferromagnetic and (b) antiferromagnetic NiO derived from periodic calculations.

Figure 9 shows the composition of the valence and conduction band features resulting from the periodic calculations of the ferromagnetic and antiferromagnetic NiO electronic structure. As found in the cluster calculations, the periodic results also show strong admixture of nickel 3d and oxygen 2p levels in the valence band region, with the top of the valence band containing significant amounts of O 2p character. The very narrow feature that comprises the bottom of the conduction band in the periodic calculations for the antiferromagnetic NiO system is reasonably well predicted by the cluster model although slightly broader. This broadening is, as stated previously, most likely due to using a finite cluster with limited numbers of orbitals (312 total electrons for the largest cluster, $Ni_{12}O_{12}$) to describe an infinite bulk electronic structure.

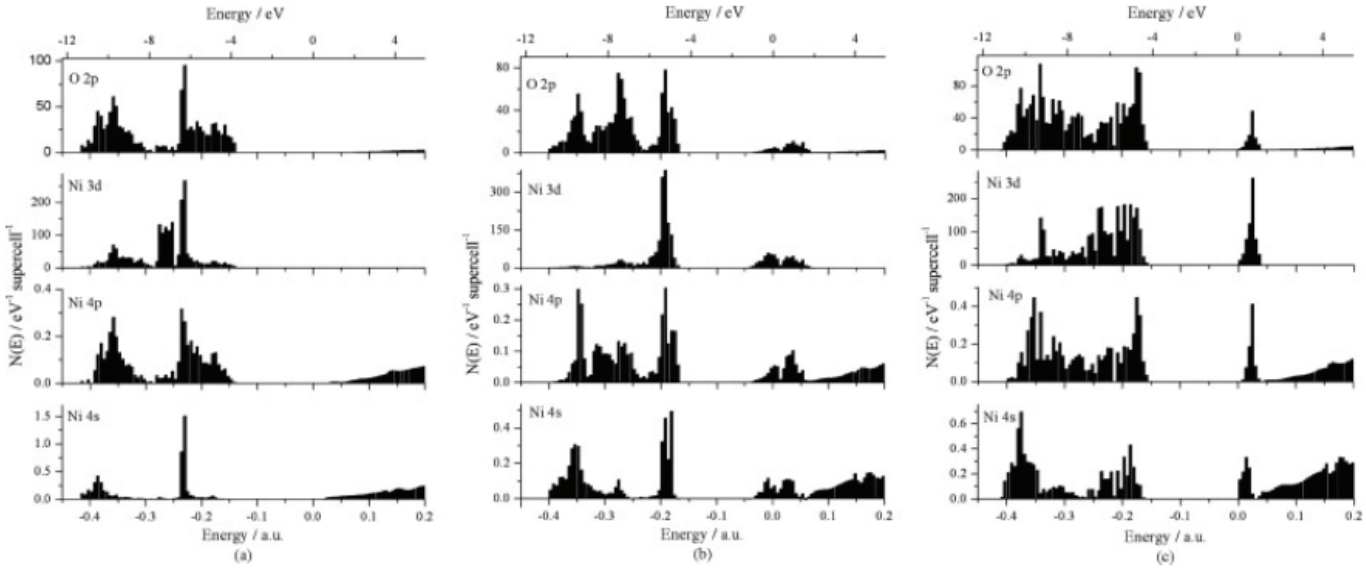

Figure 9. Projected density of states for the valence band and the lowermost part of the conduction band for (a) majority-spin α ferromagnetic, (b) minority-spin β ferromagnetic and (c) α + β antiferromagnetic NiO structures from periodic calculations.

Most significant is the agreement between periodic and cluster calculations to reproduce the character at the top of the valence band and the bottom of the conduction band. Noncontroversially, the bottom of the conduction band is comprised almost entirely of Ni 3d states. More significantly, the top of the valence band shows substantial O 2p nature although the periodic results predict a smaller contribution from the oxygen states at the top of the valence band than do the cluster calculations. Ni 3d states comprise 37% of the α subband character and 82% of the β subband within the top 1 eV of the ferromagnetic valence band, as opposed to 15-20% of the α subband and 34-42% β subband in the cluster calculations. For the antiferromagnetic NiO system, the nickel 3d contribution to the top 1 eV of the valence band structure is 66% with periodic methods but only approximately 27% with the cluster models. In both periodic and cluster calculations, only Ni 3d and O 2p states contribute significantly to the valence band, with negligible contributions from Ni 4s and Ni 2p states, and the remainder of this valence band region is predominately O 2p. Thus, the periodic calculations predict about a 50% smaller contribution from oxygen-derived states to the top of the valence band than do the cluster calculations, indicating that even the largest cluster still overestimates the hybridization between the oxygen and nickel states.

Conclusions

In this work, we propose a simple and convenient empirical method for estimating the point charge, q, for embedded cluster calculations by density functional methods appropriate for modeling transition metal oxide systems. An optimized point charge value was obtained for a series of nickel oxide clusters, Ni_xO_x (x = 4–12) by choosing q to reproduce the experimentally observed lattice parameter a. The effect of the point charge was then studied for several bulk NiO properties, including lattice energy E_{lat}, bulk modulus B, valence band gap E_g, and ionic charge Q for point charge array values of $0 \leq q \leq 2.0$. The bulk parameters are strongly dependent on the magnitude of the surrounding point charge array and reproduce experimental data quite well at the optimum point charge value, diverging significantly for smaller and larger q. The optimum value of q depends upon cluster size, decreasing as the cluster size increases, but in all cases is significantly less that the formal charge q = ±2.0 often used in embedded cluster calculations for divalent oxides. For the largest cluster studied here, $Ni_{12}O_{12}$, q = ±0.479 and 0.507 for ferromagnetic and antiferromagnetic spin ordered clusters, respectively.

The electronic structure of NiO clusters is also well reproduced for all but the smallest cluster sizes of x = 4 for ferromagnetic and x = 4 and 6 for antiferromagnetic clusters and is in general agreement with both experimental and calculated valence band structures. There is some controversy over the composition of the top of the valence band, and the present study places substantial O 2p character in this region, in agreement with a number of other computational studies. The total contribution of Ni 3d orbitals in the top 1 eV of the valence band region is only very weakly dependent of the cluster size, and is calculated to range from 26 to 30% of the total orbital content. Again, the largest change in composition occurs at small cluster size. The overall density of states shape and bandgap value are generally consistent with the results of periodic calculations, although the clusters most likely overestimate the contribution from the O 2p states to the top of the valence band.

References

1 Mott, N. F. *Proc Phys Soc London* 1949, **62**, 416.

2 Mott, N. F. *Can J Phys* 1956, **34**, 1356.

3 Austin, I. G.; Mott, N. F. *Science* 1970, **168**, 71.

4 Hubbard, J. *Proc R Soc London Ser A* 1964, **237**, 277.

5 Hubbard, J. *Proc R Soc London Ser A* 1964, **281**, 401.

6 Shen, Z. X.; Shih, C. K.; Jepsen, O.; Spicer, W. E.; Lindeau, I.; Allen, J. A. *Phys Rev Lett* 1990, **64**, 2442.

7 Sawatzky, G. A.; Allen, J. W. *Phys Rev Lett* 1984, **53**, 2339.

8 Fujimori, A.; Minami, F. *Phys Rev B* 1984, **30**, 957.

9 Hufner, S. *Adv Phys* 1994, **43**, 183.

10 Schuler, T. M.; Ederer, D. L.; Itza-Ortiz, S.; Woods, G. T.; Callcott, T. A.; Woicik, J. C. *Phys Rev B* 2005, **71**, 115113.

11 Eder, R.; Dorneich, A.; Winter, H. *Phys Rev B* 2005, **71**, 045105.

12 Bengone, O.; Alounai, M.; Hlochl, P.; Hugel, J. *Phys Rev B* 2000, **62**, 16392.

13 Hufner, S.; Hulliger, F.; Osterwalder, J.; Riesterer, T. *Solid State Commun* 1984, **50**, 83.

14 McKay, J. M.; Henrich, V. E. *Phys Rev Lett* 1984, **53**, 2343.

15 Osterwalder, J.; Riesterer, T.; Hulliger, F. *Solid State Commun* 1984, **52**, 793.

16 Hufner, S.; Riesterer, T. *Phys Rev B* 1986, **33**, 7267.

17 Cox, P. A. *Transition Metal Oxides: An Introduction to Their Electronic Structure and Properties*. *The International Series of Monographs on Chemistry*, Vol. **27**; Clarendon Press: Oxford, 1995.

18 Powell, R. J.; Spicer, W. E. *Phys Rev B* 1970, **2**, 2181.

19 Zheng, H. *Phys Rev B* 1993, **48**, 14868.

20 Neshev, N. M.; Alexiev, V. D.; Parvanov, V. M.; Mineva, T. I.; Chihaia, V.; Munteanu, G. *Bulgarian Chem Commun* 1998, **30**, 323.

21 Nagai, J.; Morisaki, S. *Solid State Ionics* 2003, **165**, 149.

22 Takahashi, H.; Munakata, F.; Yamanaka, M. *J Phys: Condens Matter* 1995, **7**, 1583.

23 Bredow, T.; Geudtner, G.; Jug, K. *J Comput Chem* 2001, **22**, 89.

24 Satitkovitchai, K.; Pavlyukh, Y.; Hubner, W. *Phys Rev B* 2003, **67**, 165413.

25 Faleev, S. V.; van Schilfgaarde, M.; Kotani, T. *Phys Rev Lett* 2004, **93**, 126406.

26 Hoeft, J. T.; Kittel, M.; Polchik, M.; Bao, S.; Toomes, R. L.; Kang, J.-H.; Woodruff, D. P.; Pascal, M.; Lamont, C. L. A. *Phys Rev Lett* 2001, **87**, 086101.

27 Kittel, M.; Hoeft, J. T.; Bao, S.; Polchik, M.; Toomes, R. L.; Kang, J.-H.; Woodruff, D. P.; Pascal, M.; Lamont, C. L. A. *Surf*

Sci 2002, **499**, 1.

28 Pacchioni, G.; Di Valentin, C.; Dominguez-Ariza, D.; Illas, F.; Bredow, T.; Kluner, T.; Staemmler, V. *J Phys: Condens Matter* 2004, **16**, S2497.

29 Di Valentin, C.; Pacchioni, G.; Bredow, T.; Dominguez-Ariza, D.; Illas, F. *J Chem Phys* 2002, **117**, 2299.

30 Bredow, T. *J Phys Chem B* 2002, **106**, 7053.

31 Evjen, H. M. *Phys Rev* 1932, **39**, 675.

32 Anderson, A. B. *Chem Phys Lett* 1980, **72**, 514.

33 Grimes, R. W.; Onwood, D. *J Chem Soc Faraday Trans* 1990, **86**, 233.

34 Xu, X.; Nakatsuji, N.; Ehara, M.; Lu, X.; Wang, N. Q.; Zhang, Q. E. *Chem Phys Lett* 1998, **292**, 282.

35 Xu, X.; Lu, X.; Wang, N. Q.; Zhang, Q. E. *Chem Phys Lett* 1995, **235**, 541.

36 Neyman, K. M.; Rosch, N. *J Mol Struct* 1993, **293**, 303.

37 Pelmenschikov, A. G.; Morosi, G.; Gamba, A. *J Phys Chem* 1995, **99**, 15018.

38 Neyman, K. M.; Rosch, N. *Surf Sci* 1993, **297**, 223.

39 Neyman, K. M.; Ruzankin, S. P.; Rosch, N. *Chem Phys Lett* 1995, **246**, 546.

40 Neyman, K. M.; Rosch, N. *Chem Phys* 1992, **168**, 267.

41 Xu, X.; Nakatsuji, H.; Lu, X.; Ehara, M.; Cai, Y.; Wang, N. Q.; Zhang, Q. E. *Theor Chem Acc* 1999, **102**, 170.

42 Xu, Y.; Li, J.; Zhang, Y.; Chen, W. *Surf Sci* 2003, **525**, 13.

43 Li, J.; Xu, Y.; Zhang, Y. *Solid State Commun* 2003, **126**, 107.

44 Frisch, M. J.; Trucks, G. W.; Schlegel, H. B.; Scuseria, G. E.; Robb, M. A.; Cheeseman, J. R.; Montgomery, J. A., Jr.; Vreven, T. K.; Kudin, N.; Burant, J.; Millam, M.; Iyengar, S. S.; Tomasi, J.; Barone, V.; Mennucci, B.; Cossi, M.; Scalmani, G.; Rega, N.; Petersson, G. A.; Nakatsuji, H.; Hada, M.; Ehara, M.; Toyota, K.; Fukuda, R.; Hasegawa, J.; Ishida, M.; Nakajima, T.; Honda, Y.; Kitao, O.; Nakai, H.; Klene, M.; Li, X.; Knox, J. E.; Hratchian, H. P.; Cross, J. B.; Adamo, C.; Jaramillo, J.; Gomperts, R.; Stratmann, R. E.; Yazyev, O.; Austin, A. J.; Cammi, R.; Pomelli, C.; Ochterski, J. W.; Ayala, P. Y.; Morokuma, K.; Voth, G. A.; Salvador, P.; Dannenberg, J. J.; Zakrzewski, V. G.; Dapprich, S.; Daniels, A. D.; Strain, M. C.; Farkas, O.; Malick, D. K.; Rabuck, A. D.; Raghavachari, K.; Foresman, J. B.; Ortiz, J. V.; Cui, Q.; Baboul, A. G.; Clifford, S.; Cioslowski, J.; Stefanov, B. B.; Liu, G.; Liashenko, A.; Piskorz, P.; Komaromi, I.; Martin, R. L.; Fox, D. J.; Keith, T.; Al-Laham, M. A.; Peng, C. Y.; Nanayakkara, A.; Challacombe, M.; Gill, P. M. W.; Johnson, B.; Chen, W.; Wong, M. W.; Gonzalez, C.; Pople, J. A. Gaussian Inc.: Wallingford, CT, 2004.

45 Becke, A. D. *J Chem Phys* 1993, **98**, 5648.

46 Lee, C.; Yang, W.; Parr, R. G. *Phys Rev B* 1988, **37**, 785.

47 Dunning, T. H., Jr.; Hay, P. J.In *Modern Theoretical Chemistry*, Vol. **3**; Schaefer, H. F. , Ed.; Plenum: New York, 1976.

48 Hay, P. J.; Wadt, W. R. *J Chem Phys* 1985, **82**, 270.

49 Francl, M. M.; Pietro, W. J.; Hehre, W. J.; Binkley, J. S.; Gordon, M. S.; DeFrees, D. J.; Pople, J. A. *J Chem Phys* 1982, **77**, 3654.

50 Simons, S.; Jorgensen, P.; Taylor, H.; Ozment, J. *J Phys Chem* 1983, **87**, 2745.

51 Cerjan, C. J.; Miller, W. H. *J Chem Phys* 1981, **75**, 2800.

52 Bannerjee, A.; Adams, N.; Simons, J.; Shepard, R. *J Phys Chem* 1985, **89**, 52.

53 Towler, M. D.; Allan, N. L.; Harrison, N. M.; Saunders, V. R.; Mackrodt, W. C.; Apra, E. *Phys Rev B* 1994, **50**, 5041.

54 Lu, X.; Xu, X.; Wang, N.; Zhang, Q.; Ehara, M.; Nakatsuji, H. *Chem Phys Lett* 1998, **291**, 445.

55 Wyckoff, R. W. G. *Crystal Structures*; Wiley: New York, 1963.

56 Pisani, C.; Dovesi, R.; Roetti, C. *Hartree-Fock Ab initio Treatment of Crystalline Systems, Lecture Notes in Chemistry*, Vol. **48**; Springer-Verlag: Heidelberg, 1988.

57 Saunders, V.; Dovesi, R.; Roetti, C.; Causà, M.; Harrison, N.; Orlando, R.; Zicovich-Wilson, C. *CRYSTAL98, User Manual*; Università di Torino and SERC Daresbury Laboratory, 1999.

58 Bredow, T.; Gerson, A. *Phys Rev B* 2000, **61**, 5194.

59 Uchida, N.; Saito, S. *J Acoust Soc Am* 1972, **51**, 1602.

60 Staemmler, V. *Top Organomet Chem* 2005, **12**, 219.

61 Kittel, C. *Intoduction to Solid State Physics*, 7th ed.; Wiley: New York, 1996.

62 Berrondo, M.; Rivas-Silva, J. F. *Int J Quant Chem* 1996, **57**, 1115.

63 Powell, R. J.; Spicer, W. E. *Phys Rev B* 1970, **2**, 2182.

64 Hufner, S. *Photoelectron spectroscopy*, 2nd ed., Vol. **82**: *Spinger Series in Solid-State-Sciences*; Springer: Berlin, 1996; p. 186.

65 Duda, L.-C.; Schmitt, T.; Magnuson, M.; Forsberg, J.; Olsson, A.; Nordgren, J.; Okada, K.; Kotani, A. *Phys Rev Lett* 2006, **96**, 067402.

66 Li, J.-L.; Rignanese, G.-M.; Louie, S. G. *Phys Rev B* 2005, **71**, 193102.

67 Hufner, S.; Werthein, G. K. *Phys Rev B* 1973, **8**, 4857.

68 de Moreira, P. R.; Illas, F.; Martin, R. L. *Phys Rev B* 2002, **65**, 155102.

69 Feng, X.-B.; Harrison, N. M. *Phys Rev B* 2004, **69**, 035114.